Nonlinear transport in an out-of-equilibrium single-site Bose-Hubbard model: Scaling, rectification, and time dynamics

Archak Purkayastha, Abhishek Dhar, and Manas Kulkarni
International Centre for Theoretical Sciences, Tata Institute of Fundamental Research, Bangalore 560089, India
(Received 26 September 2016; published 28 November 2016)

Recent experiments in hybrid-quantum systems facilitate the potential realization of one of the most fundamental interacting Hamiltonian-reservoir systems, namely the single-site Bose-Hubbard model coupled to two reservoirs at different temperatures. Using Redfield equations in a Born-Markov approximation, we compute nonequilibrium average particle number, energy, and currents beyond linear response regime, both time dynamics and steady state, and investigate its dependence on various tunable parameters analytically. We find interesting scaling laws in high-temperature regimes that are independent of choice of bath spectral functions. We also demonstrate that the system shows very interesting particle and energy current rectification properties which can be controlled via the relative strength of interaction and temperatures, as well as via the degree of asymmetry in system-bath coupling. Specifically, we find inversion of direction of energy rectification as a function of the relative strength of the interaction strength and the temperatures. We also show that, in the limit of low-temperature and high interaction strength, our results are consistent with the nonequilibrium spin-Boson model. Our results are experimentally relevant not only to hybrid quantum systems but also in other areas such as molecular junctions.

DOI: 10.1103/PhysRevA.94.052134

I. INTRODUCTION

Far-from-equilibrium systems beyond the paradigm of linear response has been a subject of growing theoretical and experimental interest [1–8]. Such studies are important from a fundamental perspective and from the point of view of device applications. In particular, understanding the role of interactions is of great interest. Important fundamental problems to explore include the role of far-from-equilibrium physics in physical quantities of interest and the intricate interplay between system and bath degrees of freedom when interactions are involved. Some of the main consequences of interactions range from fundamental physics (such as the phenomenon of the Kondo effect [9,10]) to device applications (such as diodes and rectifiers [11–13]). Even though the role of interaction in device applications in fermionic systems is well studied [14–16], the corresponding bosonic setups are much less explored. However, with the advent of the relatively new field of photonics, bosonic setups for device applications such as a potential optical diode are gaining popularity [17–19]. With recent cutting-edge technology in hybrid quantum systems, it is now possible to design interacting bosonic Hamiltonians and reservoirs [8,20–25]. There has been not only progress in fabricating Hamiltonian-reservoir systems but also great advances in measuring physical quantities of interest such as photon number, photon statistics [26], and photon current [27].

One of the most basic interacting bosonic Hamiltonian system that one can think of is a single bosonic site with Bose-Hubbard interaction, hereafter called the single-site Bose Hubbard (SSBH) model. In optics, such an interaction is often called the Kerr interaction strength. In the field of hybrid quantum systems a Hamiltonian with such an interaction can be potentially experimentally realized in more than one way. The Jaynes-Cummings model, an experimentally realized light-matter system, can be tuned to the dispersive regime where it behaves like a SSBH model. The photon-spin interaction in this limit can be integrated out "pertubatively" to generate a nonlinear Bose-Hubbard like interaction between photons [21,28]. Alternatively there are interesting potential realizations of Bose-Hubbard interactions between photons which involve four-level atoms in an optical cavity [29,30]. These realizations offer large tunability of parameters. Specifically, while the former realization involving Jaynes-Cummings model has a small interaction strength compared to the linear term, the later realizations have very large interaction strength.

Another area of applicability for such interacting bosonic Hamiltonians, which is perhaps more suited to nonequilibrium measurements, are the fields of molecular thermoelectrics and nanophononics. These fields typically deal with molecular junctions connecting two reservoirs, experimentally, which are often two large chemical compounds [31–36]. The role of interactions in phononic transport through such systems is of interest both experimentally and theoretically [37].

There has been a large amount of work on such a SSBH model with a finite interaction strength coupled to a single bath [38–43]. On the other hand, the nonequilibrium spin boson (NESB) model, which corresponds to the limit of very large interaction strength, has been well studied in out-of-equilibrium setups [10,44–48] and is of growing experimental significance. The conductance of an anharmonic junction with quartic anharmonicity has been studied recently [49,50]. However, there is essentially no investigation of the SSBH model with finite interaction strength in a far-from-equilibrium setup via connection with multiple reservoirs. In this paper, we investigate the SSBH model weakly coupled to two bosonic baths at different temperatures beyond the linear response regime.

The organization of our paper is as follows: In Sec. II, we describe our setup. In Sec. III, we give the Redfield quantum master equation for our setup and, in Sec. IV, we find the nonequilibrium steady-state (NESS) properties. In Sec. V, we look at scaling behavior of average particle number and energy

 ©2016 American Physical Society

at NESS and, in Sec. VI, we discuss the scaling behavior and rectification of NESS particle and energy currents. In Sec. VII, we present results for time dynamics of various physical quantitites, which has become of growing recent interest. Finally, in Sec. VIII, we summarize our main results along with an outlook.

II. MODEL AND SETUP

We consider a single site with Bose-Hubbard interaction connected to two bosonic baths in nonequilibrium. The baths are taken to be quadratic and the system-bath couplings are taken to be bilinear. Thus our setup is given by the full system+bath Hamiltonian

$$\begin{aligned}\hat{H} &= \hat{H}_S + \hat{H}_B + \hat{H}_{SB}\\ \hat{H}_S &= \Omega_0 \hat{a}^\dagger \hat{a} + \chi(\hat{a}^\dagger \hat{a})^2\\ \hat{H}_B &= \sum_{\ell=1}^{2}\sum_{r=1}^{\infty} \Omega_r^\ell \hat{B}_r^{\ell\dagger}\hat{B}_r^\ell,\\ \hat{H}_{SB} &= \varepsilon \sum_{\ell=1}^{2}\sum_{r} \left(\kappa_{\ell r}\hat{B}_r^{\ell\dagger}\hat{a} + \kappa_{\ell r}^* \hat{a}^\dagger \hat{B}_r^\ell\right),\end{aligned} \tag{1}$$

where $\hat{a}$ correspond to bosonic annihilation operators and $\hat{B}_r^\ell$ to those of ℓth bath ($\ell = \{1,2\}$). Note that $\hat{N} = \hat{a}^\dagger\hat{a}$ is a conserved quantity with respect to the system Hamiltonian H_S. The energy spectrum of the system Hamiltonian can be easily written down and it has the nonlinear form $\hat{E} = \Omega_0\hat{N} + \chi\hat{N}^2$.

The baths are quadratic and have infinite degrees of freedom. ε is a dimensionless parameter that controls system bath coupling. We assume that, initially, there is no coupling between the system and the baths, and the two baths are at thermal equilibrium with their own inverse temperature β_1 and β_2 and chemical potential μ_1 and μ_2. Thus the initial bath correlation functions satisfy the thermal properties:

$$\left\langle \hat{B}_r^\ell \right\rangle = 0, \quad \left\langle \hat{B}_r^{\ell\dagger}\hat{B}_s^\ell \right\rangle_B = \mathfrak{n}_\ell\left(\Omega_r^\ell\right)\delta_{rs}, \tag{2}$$

where $\mathfrak{n}_\ell(\omega) = [e^{\beta_\ell(\omega-\mu_\ell)} - 1]^{-1}$ is the bosonic distribution function. We also introduce the bath spectral functions:

$$\mathcal{J}_\ell(\omega) = 2\pi \sum_r |\kappa_{\ell r}|^2 \delta\left(\omega - \Omega_r^\ell\right). \tag{3}$$

We will assume

$$\mathcal{J}_\ell(\omega) = \Gamma_\ell \mathcal{J}(\omega), \tag{4}$$

i.e., the two baths have same density of states, but the system-bath coupling differs in general. Γ_ℓ has dimensions such that $\mathcal{J}_\ell(\omega)$ has dimensions of energy.

The quantitative nature of the results will depend on our choice of spectral function. We assume a general spectral function which is commonly used in bosonic systems:

$$\mathcal{J}(\omega) = \omega^s e^{-\omega/\omega_c}, \tag{5}$$

where ω_c gives the cutoff frequency. The cutoff frequency is considered very large so the system energy levels near the edge of the bath spectrum correspond to extremely high energies, which do not really contribute to the system properties at the chosen set of temperatures and chemical potentials. This is satisfied when $\omega_c \gg \Omega_0, \chi, \beta_1^{-1}, \beta_2^{-1}, \mu_1, \mu_2$. Also, we are concerned with a photonic or phononic system, so we will set $\mu_1 = \mu_2 = 0$ finally.

III. THE QUANTUM MASTER EQUATION

We want to investigate this setup without any restrictions on the interaction strength χ. So, we adopt the method of the quantumm master equation (QME) under the Born-Markov approximation, which is only valid when system-bath coupling is weak and gives results only to leading order in system-bath coupling. The microscopically derived Redfield QME for our system coupled to single bath was first written down in Ref. [39]. It is straighforward to generalize to two baths. Let us define $\hat{\rho} \equiv \mathrm{Tr}_B(\hat{\rho}_{\mathrm{full}})$ with $\hat{\rho}_{\mathrm{full}}$ being the full density matrix of system+bath and $\mathrm{Tr}_B(..)$ implying trace taken over bath degrees of freedom. The weak-coupling Redfield equation for the density matrix of the system $\hat{\rho}$ of our setup is given by

$$\frac{\partial\hat{\rho}}{\partial t} = i[\hat{\rho}, \hat{H}_S] - \varepsilon^2([\hat{\rho}F(\hat{\tilde{\omega}})\hat{a}, \hat{a}^\dagger] + [\hat{a}^\dagger, G(\hat{\tilde{\omega}})\hat{a}\hat{\rho}] + \mathrm{H.c.}), \tag{6}$$

where

$$\begin{aligned}\hat{\tilde{\omega}} &= \Omega_0 + \chi(2\hat{N} + 1),\\ F(\hat{\tilde{\omega}}) &= F_1(\hat{\tilde{\omega}}) + F_2(\hat{\tilde{\omega}}), \quad G(\hat{\tilde{\omega}}) = G_1(\hat{\tilde{\omega}}) + G_2(\hat{\tilde{\omega}})\\ F_\ell(\hat{\tilde{\omega}}) &= \frac{1}{2}\mathcal{J}_\ell(\hat{\tilde{\omega}})\mathfrak{n}_\ell(\hat{\tilde{\omega}}) - i\mathcal{P}\int_{-\infty}^{\infty}\frac{d\omega}{2\pi}\frac{\mathcal{J}_\ell(\omega)\mathfrak{n}_\ell(\omega)}{\omega - \hat{\tilde{\omega}}}\\ G_\ell(\hat{\tilde{\omega}}) &= \frac{1}{2}\mathcal{J}_\ell(\hat{\tilde{\omega}})(\mathfrak{n}_\ell(\hat{\tilde{\omega}})+1) - i\mathcal{P}\int_{-\infty}^{\infty}\frac{d\omega}{2\pi}\frac{\mathcal{J}_\ell(\omega)(\mathfrak{n}_\ell(\omega)+1)}{\omega - \hat{\tilde{\omega}}}\end{aligned} \tag{7}$$

and H.c. stands for Hermitian conjugate. Note that the Redfield equation assumes $\varepsilon \ll 1$ and keeps terms only up to $O(\varepsilon^2)$, i.e., only up to quadratic in system-bath coupling (the Born approximation). In deriving the above equation, we have also done the Markov approximation which assumes that the observation time is much larger than the time scale of relaxation of bath correlation functions. To ensure weak system-bath coupling, we choose $\varepsilon = 0.1$ and $\kappa_{\ell r}$ to be of the same order as Ω_0.

The Markov assumption entails that Eq. (6) is not valid at short times. In fact, as pointed out in Ref. [42], this equation is not completely positive and may lead to unphysical states at small times for certain initial conditions. A way around suggested in Ref. [42] is to derive Lindblad equation in terms of eigenbasis operators of $\hat{H}_S$ via the secular approximation. The equation so derived respects complete positivity at all times. In the following, we will be interested only in the diagonal elements of $\hat{\rho}$ in the eigenbasis of $\hat{H}_S$. It turns out that the evolution equation for these elements as derived from the Redfield equation and from the eigenbasis Lindblad equation are exactly the same.

In equilibrium, i.e., when $\beta_1 = \beta_2 = \beta$, $\mu_1 = \mu_2 = \mu$, it can be checked by direct substitution that the thermal state

$$\hat{\rho}_{eq} = \frac{e^{-\beta(\hat{H}_S - \mu\hat{N})}}{Z} \tag{8}$$

is the steady state of the Eq. (6), where $Z = \mathrm{Tr}[e^{-\beta(\hat{H}_S - \mu\hat{N}}]$ is the equilibrium partition function.

IV. THE NONEQUILIBRIUM STEADY STATE (NESS)

To calculate various physical observables in NESS beyond linear response, we need to find the NESS density matrix. Also, in nonequilibrium, since we have no guess for direct substitution, we need to find the ρ directly from Eq. (6). Since both the number operator $\hat{N}$ and the system Hamiltonian H_S are diagonal in occupation number basis, the NESS transport properties as well as average occupation and energy of the system can be found from the steady-state diagonal elements of $\hat{\rho}$ in this basis. The occupation number basis satisfies

$$\hat{a}|n\rangle = \sqrt{n}|n-1\rangle, \quad \hat{a}^\dagger|n\rangle = \sqrt{n+1}|n+1\rangle. \tag{9}$$

The evolution equation for the diagonal elements $\rho_n = \langle n|\hat{\rho}|n\rangle$ is given by

$$\frac{d\rho_n}{dt} = -\varepsilon^2[\rho_n(C_n + D_n) - \rho_{n-1}C_{n-1} - \rho_{n+1}D_{n+1}], \tag{10}$$

where

$$\begin{aligned} C_n &= C_n^{(1)} + C_n^{(2)}, \quad D_n = D_n^{(1)} + D_n^{(2)} \\ C_n^{(\ell)} &= (n+1)\mathcal{J}_\ell(\omega_n)\mathfrak{n}_\ell(\omega_n), \\ D_n^{(\ell)} &= n\mathcal{J}_\ell(\omega_{n-1})[\mathfrak{n}_\ell(\omega_{n-1}) + 1] \\ \omega_n &= \Omega_0 + \chi(2n+1). \end{aligned} \tag{11}$$

Inthe steady state we set the left-hand side of Eq. (10) to zero. This leads to a difference equation. Noting that $C_{-1}^{(\ell)} = C_{-1} = 0$, $D_0^{(\ell)} = D_0 = 0$, we obtain, by recursion, the solution

$$\rho_n D_n = \rho_{n-1}C_{n-1} \tag{12}$$

$$\Rightarrow \rho_n = \rho_0 \prod_{p=1}^{n} \frac{C_{p-1}}{D_p} = \rho_0 \prod_{p=1}^{n} \frac{\sum_{\ell=1}^{2}\Gamma_\ell\mathfrak{n}_\ell(\omega_{p-1})}{\sum_{\ell=1}^{2}\Gamma_\ell[\mathfrak{n}_\ell(\omega_{p-1})+1]}$$

$$\text{for } n = 1,2,3,\ldots. \tag{13}$$

The constant ρ_0 is fixed from the normalization condition $\sum_n \rho_n = 1$, i.e., the trace of the density matrix is unity. Thus,

$$\rho_0 = \tilde{Z}^{-1} = \left[1 + \sum_{n=1}^{\infty}\prod_{p=1}^{n} \frac{\sum_{\ell=1}^{2}\Gamma_\ell\mathfrak{n}_\ell(\omega_{p-1})}{\sum_{\ell=1}^{2}\Gamma_\ell(\mathfrak{n}_\ell(\omega_{p-1})+1)}\right]^{-1}, \tag{14}$$

where $\tilde{Z}$ is a normalization constant and is analogous to the partition function in equilibrium systems. It can be easily checked by putting $\mathfrak{n}_1(\omega) = \mathfrak{n}_2(\omega) = \mathfrak{n}(\omega)$ in Eq. (13) that ρ_n indeed gives Eq. (8) in equilibrium. Also, in the equilibrium case, Eq. (12) corresponds to the detailed balance condition. In the nonequilibrium case, while this still looks like the detailed balance condition, we note that in general it is not possible to define an effective temperature. Also note that ρ_n is independent of the choice of spectral function of the bath.

The explicit expression for population ρ_n of bosons in NESS, given by Eq. (13), is the central result that allows us to go beyond linear response in this interacting bosonic problem. The population, in itself, is a physically measurable quantity and, as we show below, can be used to compute various other physical observables.

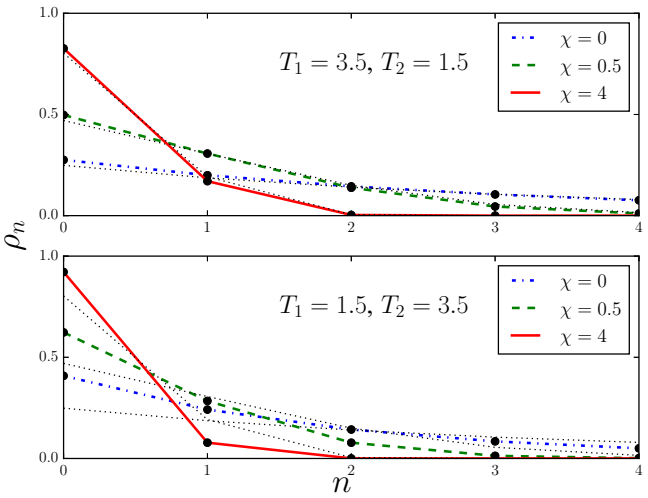

FIG. 1. The plot of population density (diagonal elements of density matrix in eigenbasis of system Hamiltonian) of SSBH model in equilibrium and under thermal bias with assymetric system-bath coupling ($\Gamma_1 = 0.4, \Gamma_2 = 1.6$) and $\Omega_0 = 1$. The top and bottom panels are for interchanged hot and cold baths. The three dotted lines (in each plot) are the corresponding equilibrium distributions ($T_1 = T_2 = 3.5$), i.e., Eq. (8) for the values of χ mentioned in the legend. The deviation from equilibrium is more prominent in the bottom panel. For large interaction strength ($\chi = 4$), only two levels have non-negligible probability, like a spin-boson model. All energy variables are measured in units of Ω_0.

In Fig. 1, we show the plots of population density ρ_n of the system under asymmetric system-bath coupling. Since system-bath coupling is asymmetric, the out-of-equilibrium distribution changes under interchange of hot and cold baths. For high interaction strength, i.e., for $\chi \gg \Omega_0, T_1, T_2$, only the lowest two levels have non-negligible probability. In this regime, we can truncate the energy spectrum in just two levels. Then ρ_0 and ρ_1 become

$$\rho_0 \approx \frac{\sum_{\ell=1}^{2}\Gamma_\ell[\mathfrak{n}_\ell(\omega_0)+1]}{\sum_{\ell=1}^{2}\Gamma_\ell[1+2\mathfrak{n}_\ell(\omega_0)]}, \quad \rho_1 \approx \frac{\sum_{\ell=1}^{2}\Gamma_\ell\mathfrak{n}_\ell(\omega_0)}{\sum_{\ell=1}^{2}\Gamma_\ell[1+2\mathfrak{n}_\ell(\omega_0)]} \quad \forall\, \chi \gg \Omega_0, T_1, T_2 \tag{15}$$

with $\omega_0 = \Omega_0 + \chi$. The above results are exactly the same as obtained for a nonequilibrium spin-boson model (NESB) by using the Redfield equation [44]. Thus for $\chi \gg \Omega_0, T_1, T_2$, the system becomes identical to the NESB. Since NESB is already a well-explored problem, in the following, we will be mainly interested in the physics beyond this regime. We also note that for $\chi = 0$ the system reduces to a harmonic oscillator and, in this case, the population $\rho_n^{\chi=0}$ is given in terms of an effective temperature $T_{\text{eff}} = 1/\beta_{\text{eff}}$, i.e., $\rho_n^{\chi=0} \propto e^{-\beta_{\text{eff}}\Omega_0 n}$, with

$$\coth(\beta_{\text{eff}}\Omega_0) = \frac{\Gamma_1\coth(\beta_1\Omega_0) + \Gamma_2\coth(\beta_2\Omega_0)}{\Gamma_1 + \Gamma_2}, \tag{16}$$

which is consistent with the finding in Ref. [51].

V. AVERAGE OCCUPATION AND ENERGY

First, we will look at the average occupation and energy of the system. These quantities are measurable in current

state-of-the-art experiments in quantum light-matter hybrid systems [21,26]. The expressions for these are given by

$$\langle \hat{N} \rangle = \sum_{n=1}^{\infty} n\rho_n = \frac{1}{\tilde{Z}} \sum_{n=1}^{\infty} n \prod_{p=1}^{n} \frac{\sum_{\ell=1}^{2} \Gamma_\ell \mathfrak{n}_\ell(\omega_{p-1})}{\sum_{\ell=1}^{2} \Gamma_\ell(\mathfrak{n}_\ell(\omega_{p-1})+1)},$$
$$\langle \hat{H}_S \rangle = \sum_{n=1}^{\infty} E_n\rho_n = \frac{1}{\tilde{Z}} \sum_{n=1}^{\infty} E_n \prod_{p=1}^{n} \frac{\sum_{\ell=1}^{2} \Gamma_\ell \mathfrak{n}_\ell(\omega_{p-1})}{\sum_{\ell=1}^{2} \Gamma_\ell[\mathfrak{n}_\ell(\omega_{p-1})+1]}, \tag{17}$$

with $E_n = \Omega_0 n + \chi n^2$.

In the NESB limit, these average quantities can be trivially found from Eq. (15). They become $\langle \hat{N} \rangle \approx \rho_1$ and $\langle \hat{H}_S \rangle \approx \omega_0 \rho_1$. We are interested in going beyond the NESB regime. So let us look at the regime of high temperatures $T_1, T_2 \gg \chi, \Omega_0$. First, we look at the normalization constant defined in Eq. (14). which can be written as

$$\tilde{Z} = 1 + \sum_{n=1}^{\infty} \exp\left\{ -\sum_{p=1}^{n} \log[f(\omega_{p-1})] \right\}$$
$$f(\omega_p) = \frac{\sum_{\ell=1}^{2} \Gamma_\ell[\mathfrak{n}_\ell(\omega_p)+1]}{\sum_{\ell=1}^{2} \Gamma_\ell \mathfrak{n}_\ell(\omega_p)}. \tag{18}$$

Note that $f(\omega_p) > 1$, and hence $\log[f(\omega_p)] > 0$. It follows that there is an energy level cutoff n^* beyond which the energy levels have negligible contribution to $\tilde{Z}$. For high-enough temperatures, we can assume, $\beta_\ell \omega_p \ll 1 \; \forall p < n^*$. Under this condition, we can expand $f(\omega_p)$ to obtain (after some amount of algebra),

$$f(\omega_p) \approx 1 + \frac{\omega_p}{\tilde{T}},$$
$$\text{hence } \log[f(\omega_p)] \approx \log\left(1 + \frac{\omega_p}{\tilde{T}}\right) \approx \frac{\omega_p}{\tilde{T}}, \tag{19}$$

with

$$\tilde{T} = \frac{\Gamma_1 T_1 + \Gamma_2 T_2}{\Gamma_1 + \Gamma_2}. \tag{20}$$

The contribution of terms $n > n^*$ is small and so their precise form is irrelevant. Hence we get

$$\tilde{Z} \approx 1 + \sum_{n=1}^{\infty} \exp\left\{ -\frac{1}{\tilde{T}} \sum_{p=1}^{n} [\Omega_0 + (2p-1)\chi] \right\}$$
$$= \sum_{n=0}^{\infty} \exp\left[-\frac{1}{\tilde{T}} (\Omega_0 n + \chi n^2) \right]. \tag{21}$$

Thus, for $T_1, T_2 \gg \Omega_0, \chi$, the normalization constant has the same form as the equilibrium partition function with the effective temperature $\tilde{T}$. This is consistent with the effective temperature for harmonic oscillator ($\chi = 0$) given in Eq. (16). For high temperatures, $\beta_{\text{eff}} = 1/\tilde{T}$. It is also interesting to note that for symmetric system-bath coupling, i.e., $\Gamma_1 = \Gamma_2$, the effective temperature is just the mean temperature, $\tilde{T} = T_m = (T_1 + T_2)/2$. However, the description in terms of an effective temperature is not possible for low temperatures, except when $\chi = 0$.

The high-temperature scaling of the normalization constant can now be easily found by noting that, for high temperatures, the summation can be converted into an integral. So we have

$$\tilde{Z} \approx \int_0^{\infty} dx \exp\left[-\frac{1}{\tilde{T}} (\Omega_0 x + \chi x^2) \right] \approx \frac{\sqrt{\pi}}{2} \sqrt{\frac{\tilde{T}}{\chi}}. \tag{22}$$

The second step requires the condition $\tilde{T}\chi \gg \Omega_0^2$, under which we see that the normalization constant scales as $\sqrt{\tilde{T}/\chi}$.

The above trick can be used to find high-temperature scaling of the average of any operator which is diagonal in the eigenbasis of the system Hamiltonian. The average of any operator $\hat{h}$ which is diagonal in the eigenbasis of the system has the form

$$\langle \hat{h} \rangle = \sum_{n=0}^{\infty} \rho_n h(n) = \frac{\left\{ h(0) + \sum_{n=1}^{\infty} e^{-\sum_{p=1}^{n} \log[f(\omega_{p-1})]} h(n) \right\}}{\tilde{Z}}, \tag{23}$$

which, for $T_1, T_2 \gg \Omega_0, \chi$, exactly following the above arguments, becomes

$$\langle \hat{h} \rangle \approx \frac{\sqrt{2}}{\pi} \sqrt{\frac{\chi}{\tilde{T}}} \int_0^{\infty} dx \exp\left[-\frac{\Omega_0 x + \chi x^2}{\tilde{T}} \right] h(x). \tag{24}$$

Using this, we readily obtain the high-temperature behavior of $\langle \hat{N} \rangle$ and $\langle \hat{H}_S \rangle$,

$$\langle \hat{N} \rangle \approx \sqrt{\frac{\tilde{T}}{\pi\chi}}, \quad \langle \hat{H}_S \rangle \approx \tilde{T} + (\Omega_0 + 2\chi)\sqrt{\frac{\tilde{T}}{\pi\chi}}. \tag{25}$$

Thus $\langle \hat{N} \rangle$ should show a data collapse for various χ and vary as a function of $\sqrt{\tilde{T}/\chi}$, whereas $\langle \hat{H}_S \rangle/\chi$ varies as $\tilde{T}/\chi$ and should show a data collapse for $\chi \gg \Omega_0$.

To check the above high-temperature discussion and the connection with equilibrium behavior, we now first define

$$r = \frac{T_2}{T_1}, \tag{26}$$

which quantifies the degree of deviation from equilibrium, with $r = 1$ corresponding to equilibrium. To ensure that the system is far from equilibrium, we keep r fixed at $r < 1$. We note that if r is kept fixed, all the NESS results become a function of only one temperature, say, T_1. We choose T_1/ω_0, where $\omega_0 = \Omega_0 + \chi$, as the scaling variable since it can be used both in the highly interacting regime (where $\chi \approx \omega_0$) and the linear regime (where $\chi = 0$). Also in the NESB regime, with r fixed, all NESS quantities vary as a function of T_1/ω_0, as can be checked from Eq. (15).

In Fig. 2, we plot $\langle \hat{N} \rangle$ and $\langle \hat{H}_S \rangle/\omega_0$ as a function of T_1/ω_0. Note that Eq. (17), and not any simplified expression, was used to calculate $\langle \hat{N} \rangle$ and $\langle \hat{H}_S \rangle$ in the plots. The plots clearly show data collapse over the entire temperature regime for $\chi \gg \Omega_0$. Also important to note is the substantial effect of small interaction strengths at high temperatures. The high-temperature scaling behavior for small interaction strengths is the same as that for large interaction strengths, but there is no data collapse. This is because the condition $\tilde{T}\chi \gg \Omega_0^2$ means that, for small χ, there are large subleading terms. The low-temperature behavior matches with NESB. Since all these observations are valid for any choice of r, it follows that they

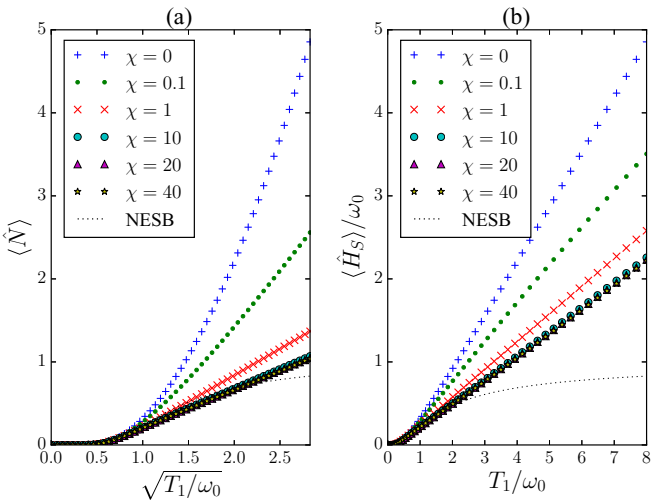

FIG. 2. The plot shows scaling behavior of average occupation and average energy of the single-site Bose-Hubbard model for fixed $r = T_2/T_1 = 1/3$. Here $\omega_0 = \Omega_0 + \chi$. The dotted plots correspond to the NESB model. For $\chi \gg \Omega_0$ ($\Omega_0 = 1$), there is data collapse over the entire range of temperatures. Even for small $\chi (= 0.1)$, there is substantial deviation from linear ($\chi = 0$) behavior. For high temperatures, $\langle \hat{N} \rangle$ scales as $\sqrt{T_1/\omega_0}$, while, $\langle \hat{H}_S \rangle$ scales as T_1. Here the system-bath coupling is taken as symmetric: $\Gamma_1 = \Gamma_2 = 1$. All energy variables are measured in units of Ω_0.

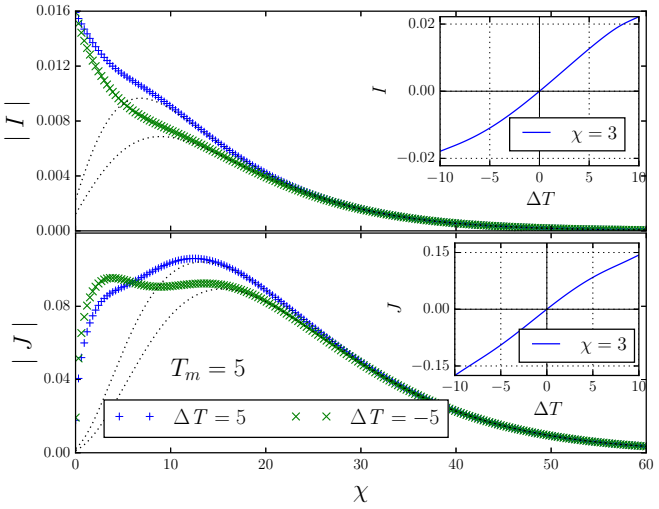

FIG. 3. Plot of particle (top panel) and energy (bottom panel) currents as a function of interaction strength χ for transport under both forward and backward bias for Ohmic baths [$s = 1$ in Eq. (5)] under asymmetric system bath coupling ($\Gamma_1 = 0.4, \Gamma_2 = 1.6$). Here the mean temperature $T_m = (T_1 + T_2)/2 = 5$ for both plots. The two black dotted lines in each plot correspond to the NESB currents for $\Delta T = \pm 5$. The currents from our model match the NESB currents for large χ. Particle current decreases with χ, while energy current behaves nonmonotonically with χ. The forward and backward currents do not match, thereby showing rectification effect. The direction of rectification of energy current is reversed beyond a value of χ. It follows that at this value of χ, the energy current does not show rectification. The insets show the corresponding currents as a function of $\Delta T = T_1 - T_2$ for a chosen value of $\chi = 3$ and $T_m = 5$. It can be seen that I and J deviate from odd-function behavior, which is a signature of rectification. Other parameters are $\varepsilon = 0.1, \omega_c = 1000$. All energy variables are measured in units of Ω_0, and time is measured in units of Ω_0^{-1}.

also are all valid in equilibrium (i.e., $r = 1$). This is consistent with previous results in Ref. [39].

The crucial point in the above discussion was to find that high-temperature nonequilibrium results can be described via an effective temperature $\tilde{T}$. In the following, we will see that even transport properties at high temperatures can be described in terms of $\tilde{T}$.

VI. CURRENTS

Now we look at the average transport properties of the system; in particular, we compute particle and energy currents. To calculate current, we look at the evolution equations of the expectation values $\langle \hat{N} \rangle$ and $\langle \hat{H}_S \rangle$ of $\hat{N}$ and H_S. Since $\hat{N}$ and $\hat{H}_S$ are diagonal in the eigenbasis of the system Hamiltonian, we can directly obtain the evolution of their expectation values from Eq. (10). This gives

$$\frac{d\langle \hat{N} \rangle}{dt} = \sum_n n \frac{d\rho_n}{dt} = \varepsilon^2 \sum_n (\rho_n C_n - \rho_n D_n), \tag{27}$$

$$\frac{d\langle \hat{H}_S \rangle}{dt} = \sum_n (\Omega_0 n + \chi n^2) \frac{d\rho_n}{dt} = \varepsilon^2 \sum_n (\omega_n \rho_n C_n - \omega_{n-1} \rho_n D_n). \tag{28}$$

Collecting all terms depending on each bath separately, the above equations can be written like continuity equations of the forms $d\langle \hat{N} \rangle/dt = I_1 - I_2, d\langle \hat{H}_S \rangle/dt = J_1 - J_2$, where I_ℓ (J_ℓ) is the particle (energy) current flowing into the system from ℓth bath. In steady state, $I_1 = I_2 = I$ and $J_1 = J_2 = J$. The steady-state expressions for currents are as follows:

$$I = \varepsilon^2 \sum_{n=0}^{\infty} \rho_n \left[C_n^{(1)} - D_n^{(1)} \right] = \sum_{n=1}^{\infty} \rho_n n \mathcal{I}(\omega_{n-1}),$$

$$J = \varepsilon^2 \sum_{n=0}^{\infty} \rho_n \left[\omega_n C_n^{(1)} - \omega_{n-1} D_n^{(1)} \right] = \sum_{n=1}^{\infty} \rho_n \omega_{n-1} n \mathcal{I}(\omega_{n-1}), \tag{29}$$

with

$$\mathcal{I}(\omega_{n-1}) = \varepsilon^2 \left\{ \frac{\Gamma_1 \Gamma_2 \mathcal{J}(\omega_{n-1}) [\mathfrak{n}_1(\omega_{n-1}) - \mathfrak{n}_2(\omega_{n-1})]}{\Gamma_1 \mathfrak{n}_1(\omega_{n-1}) + \Gamma_2 \mathfrak{n}_2(\omega_{n-1})} \right\}. \tag{30}$$

The second steps of Eq. (29) have been arrived at from the first steps after some simplification using the property of NESS density matrix given in Eq. (12). Note that energy and particle currents are not independent. But, in general, there is no way of directly finding one current given the other and they can have quite different behavior. Figure 3 shows variation of energy and particle currents with interaction strength χ for Ohmic baths [$s = 1$ in Eq. (5)] for both forward ($\Delta T > 0$) and backward ($\Delta T < 0$) biases. The mean temperature $T_m = (T_1 + T_2)/2$ is kept fixed in the plots, and system-bath coupling is asymmetric

($\Gamma_1 \neq \Gamma_2$). The plots immediately show us a number of physical aspects of the system.

First, we note that the particle current decreases with increase in interaction strength χ. This is expected because of increasing repulsive interaction in the system. On the other hand, energy current shows nonmonotonic behavior with χ. This is plausible because, while, with increasing χ, the system allows fewer particles to pass, higher-energy particles have a larger probability to pass through the system.

Second, we see that there is rectification of both energy and particle currents, since the particle and energy currents for forward and backward biases do not match. This is to be expected because the expressions for currents in Eq. (29) are not antisymmetric under interchange of hot and cold baths (i.e., $\mathfrak{n}_1 \leftrightarrow \mathfrak{n}_2$) in general. It is only so under special conditions. Two of such special conditions where there is no rectification are when $\chi = 0$, i.e., when the system is linear, and when $\Gamma_1 = \Gamma_2$ (for any χ). These can be easily checked from the expressions for currents [Eq. (29)]. Hence, in general, there will be rectification effects in both particle and energy currents for $\chi \neq 0$ and $\Gamma_1 \neq \Gamma_2$. This is the generic behavior in nonlinear (interacting) systems.

Third, as discussed above, for $\chi \gg \Omega_0, T_1, T_2$, the system behaves as NESB, and currents match with the NESB results. But, the rectification in the NESB limit is less than that for smaller interaction strengths. Thus rectification behavior is nonmonotonic as a function of χ. Our findings therefore suggest that a careful engineering of the system Hamiltonian is required to get maximum rectification from a given system.

Finally, and most interestingly, for small interaction strength, the rectification of energy current occurs in the opposite direction to rectification of particle current. Also, there is a nonzero value of χ where the forward and backward energy currents match, and hence there is no rectification. At this point, the system rectifies particle current but not the energy current. Beyond this value of χ, energy and particle rectification occur in the same direction (see Fig. 3, bottom panel).

In what follows, we investigate the behavior of particle and energy currents and rectification in more detail along with their scaling behavior.

A. Scaling behavior of currents

As we have seen with average system properties, transport properties also behave differently for different relative values of temperatures and interaction strengths. In the NESB regime, $\chi \gg \Omega_0, T_1, T_2$, the currents are given by

$$I_{SB} \approx \frac{\varepsilon^2 \Gamma_1 \Gamma_2 \mathcal{J}(\omega_0)[\mathfrak{n}_1(\omega_0) - \mathfrak{n}_2(\omega_0)]}{\Gamma_1[1 + 2\mathfrak{n}_1(\omega_0)] + \Gamma_2[1 + 2\mathfrak{n}_2(\omega_0)]},$$
$$J_{SB} \approx \omega_0 I_{SB}, \tag{31}$$

with $\omega_0 = \Omega_0 + \chi$. This is identical to the expression for current previously derived for NESB [44]. Note that in the NESB regime, energy current is proportional to particle current. This is because, in this limit, transport is allowed through transfer of exactly one particle through the system, and that particle has energy $\Omega_0 + \chi$. This is not valid beyond the NESB regime.

Now, let us look at the high-temperature regime, $T_1, T_2 \gg \chi, \Omega_0$, where the NESB results are not valid. We note that the expression for the currents in Eq. (29) has the same form as Eq. (23). So, the high-temperature trick in Eq. (24) can be readily applied to obtain

$$I^{\tilde{T} \gg \Omega_0, \chi} \approx \sqrt{\frac{2\chi}{\pi^2 \tilde{T}}} \int_0^\infty dx e^{-\frac{\Omega_0 x + \chi x^2}{\tilde{T}}} (x+1) \mathcal{I}(\omega_x),$$
$$\approx \sqrt{\frac{2\chi}{\pi^2 \tilde{T}}} \int_0^\infty dx e^{-\frac{\Omega_0 x + \chi x^2}{\tilde{T}}} (x+1) A \mathcal{J}(\omega_x) \frac{\Delta T}{\tilde{T}},$$
$$J^{\tilde{T} \gg \Omega_0, \chi} \approx \sqrt{\frac{2\chi}{\pi^2 \tilde{T}}} \int_0^\infty dx e^{-\frac{\Omega_0 x + \chi x^2}{\tilde{T}}} (x+1) \omega_x A \mathcal{J}(\omega_x) \frac{\Delta T}{\tilde{T}}, \tag{32}$$

with $A = \varepsilon^2 \Gamma_1 \Gamma_2 / (\Gamma_1 + \Gamma_2)$ and $\Delta T = T_1 - T_2$. In the second step above, we have expanded the Bose distributions in $\mathcal{I}(\omega_n)$ [Eq. (30)] for high temperatures to obtain $\mathcal{I}(\omega_n) \approx A \mathcal{J}(\omega_n) \Delta T / \tilde{T}$. Using the general form of spectral function given in Eq. (5), and after some algebra, we obtain

$$I^{\tilde{T} \gg \Omega_0, \chi} \approx K(s) = \frac{A \Delta T}{\sqrt{\pi} \tilde{T}} \int_0^\infty dy \Big[y^{-\frac{1}{2}} e^{-y} \left(\sqrt{\frac{\tilde{T} y}{\chi}} + 1 \right)$$
$$\times (\Omega_0 + \chi + 2\sqrt{\tilde{T} \chi y})^s \Big],$$
$$J^{\tilde{T} \gg \Omega_0, \chi} \approx K(s+1). \tag{33}$$

For the choice of spectral function in Eq. (5), we can relate particle and energy currents via the function $K(s)$. We now look at the properties of the function $K(s)$. First, we look at the regime $\tilde{T} \gg \chi \gg \Omega_0$. In this regime, $K(s)$ becomes

$$\frac{K(s)}{\chi^{s-1} \Delta T} \approx \frac{A}{\sqrt{\pi}} \frac{\chi}{\tilde{T}} \mathcal{F}\left(\frac{\tilde{T}}{\chi}, s \right),$$
$$\text{where} \quad \mathcal{F}(z,s) = \int_0^\infty dy \left[y^{-\frac{1}{2}} e^{-y} (\sqrt{zy} + 1)(1 + 2\sqrt{zy})^s \right]. \tag{34}$$

This then gives

$$\frac{K(s)}{\chi^{s-1} \Delta T} \approx \frac{2^{s-1} A}{\sqrt{\pi}} \left(\frac{\tilde{T}}{\chi} \right)^{\frac{s-1}{2}} s \Gamma\left(\frac{s}{2} \right), \quad \forall \ \tilde{T} \gg \chi \gg \Omega_0, \tag{35}$$

where $\Gamma(x)$ is the Gamma function. We immediately make the following observations. First, for $T_1, T_2 \gg \chi \gg \Omega_0$, $K(s)/(\chi^{s-1} \Delta T)$ varies as a function of $\tilde{T}/\chi$. Thus, $I/(\chi^{s-1} \Delta T)$ and $J/(\chi^s \Delta T)$ for various values of χ should show a data collapse when plotted with $\tilde{T}/\chi$.

Second, we see $K(1) \approx A \Delta T$. It follows that for Ohmic baths [$s = 1$ in Eq. (5)] at high temperatures, particle current is independent of the interaction strength χ and one gets a linear-response-like relation $I \approx A \Delta T$, even for large temperature bias. This is consistent with the high-temperature result for a harmonic oscillator ($\chi = 0$). However, the energy current $J \sim \sqrt{\tilde{T}/\chi} \Delta T$ and shows the effect of interaction. On the other hand, for constant bath ($s = 0$), the energy current J

always satisfies the linear-response-like relation, whereas the particle current is suppressed by a factor $\sqrt{\chi/\tilde{T}}$.

Third, we note that the quantity $J/(\chi I)$ varies as a function of $\tilde{T}/\chi$ and scales as $\sqrt{\tilde{T}/\chi}$ for any s,

$$\frac{J}{\chi I} \approx \frac{\mathcal{F}(\tilde{T}/\chi, s+1)}{\mathcal{F}(\tilde{T}/\chi, s)} \approx 2\sqrt{\frac{\tilde{T}}{\chi}}\,\frac{(s+1)\Gamma\left(\frac{s+1}{2}\right)}{s\Gamma\left(\frac{s}{2}\right)} \quad \forall\, T_1, \quad T_2 \gg \chi \gg \Omega_0. \tag{36}$$

In the other regime, $T_1, T_2 \gg \Omega_0 \gg \chi$, the scaling behavior is the same, but the data collapse is difficult to see because of large subleading terms.

Note that $I/\Delta T$ and $J/\Delta T$ actually give the *beyond linear response* analog of particle and energy conductance. For linear response, $\tilde{T} = T$ in the right-hand side of Eq. (34), T being the equilibrium temperature. Then, the above discussion gives the high-temperature scaling of conductance.

In Fig. 4, we show the scaling behavior of $I/\Delta T$ and $J/\Delta T$ as a function of T_1/ω_0. As in Sec. V, we have chosen T_1/ω_0 as the relevant scaling variable and have kept r fixed at $r < 1$ to ensure beyond linear response regime. $r \to 1$ gives the linear response conductance. The plots in Figs. 4(a) and 4(b) are then the beyond-linear-response equivalent of temperature scaling of conductance. Note that Eq. (29) (and not any simplified expression) was used to calculate currents. The plots show the scaling behavior discussed above. The plots for $\chi \gg \Omega_0$ show data collapse over the entire range of temperatures. Also, the low-temperature behavior is given by NESB.

In Fig. 4(a), we plot $I/\Delta T$ for fixed r for Ohmic baths [$s = 1$ in Eq. (5)]. We see that, for NESB, this quantity behaves nonmonotonically with temperature, while for our nonequilibrium SSBH model, this quantity monotonically increases with temperature. In fact, the deviation from NESB result starts precisely at the point where the NESB result reaches a maximum. Similar behavior is observed for $J/(\Delta T\omega_0)$ in Fig. 4(b). We conclude that the nonmonotonic behavior of

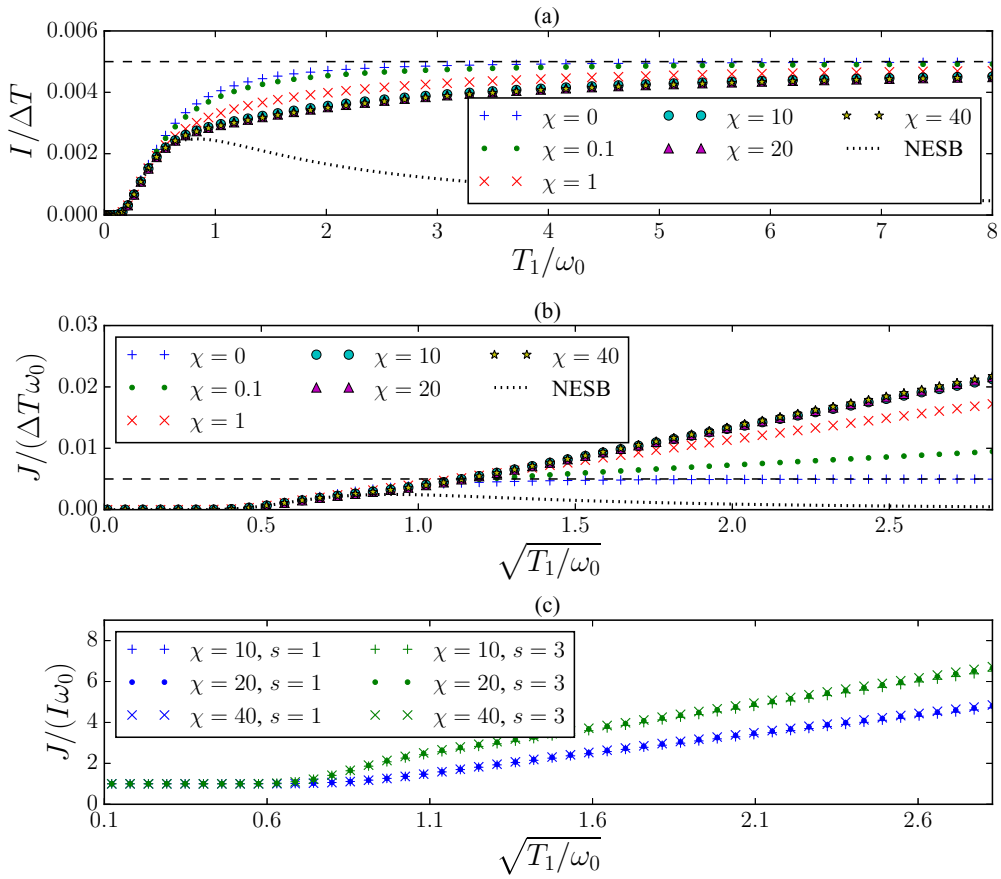

FIG. 4. Panel (a) and (b) show the scaling behavior of $I/\Delta T$ and $J/(\Delta T\omega_0)$ for Ohmic baths [$s = 1$ in Eq. (5)] and for fixed $r = \frac{T_2}{T_1} = \frac{1}{3}$. The dotted lines show the corresponding NESB result. The horizontal dashed lines in panel (a) and panel (b) correspond to $I/\Delta T = J/(\Delta T\omega_0) = A = \varepsilon^2\Gamma_1\Gamma_2/(\Gamma_1+\Gamma_2)$, which is the high-temperature result for the harmonic oscillator ($\chi = 0$). For $\chi \gg \Omega_0$ ($\Omega_0 = 1$), there is a data collapse for all temperatures. The NESB result matches with the nonequilibrium SSBH model for small temperatures. At higher temperatures, the NESB result shows nonmonotonicity, which is not seen in the nonequilibrium SSBH model which demonstrates a stark difference between the two models. In panel (a), $I/\Delta T$ approaches a constant value at high temperatures irrespective of the strength of interaction strength. In panel (b), even for small interaction strength ($\chi = 0.1$), substantial deviation from linear ($\chi = 0$) behavior is noticeable. Panel (c) shows data collapse of $J/(I\omega_0)$ for all temperatures for $\chi \gg \Omega_0$. Irrespective of choice of bath spectral function and for fixed $r(= \frac{1}{3})$, $J/(I\omega_0)$ shows a data collapse and goes as $\sim \sqrt{T_1/\omega_0}$ for $T_1 \gg \omega_0$. All observations are also valid in the linear response regime (i.e., $r \approx 1$) and give the temperature scaling of conductance. Other parameters are as follows: $\varepsilon = 0.1$, $\omega_c = 1000$, $\Gamma_1 = \Gamma_2 = 1$. All energy variables are measured in units of Ω_0, and time is measured in units of Ω_0^{-1}.

conductance of NESB, both at and beyond linear response, comes as a result of truncation of the energy spectrum and is not observed when all energy levels are considered. This demonstrates a major difference between the high-temperature behavior of nonequilibrium SSBH model and the NESB model.

Also, it follows from Fig. 4(a) that, for Ohmic baths [$s = 1$ in Eq. (5)], at high temperatures the particle current (for fixed ΔT) becomes independent of both interaction strength and the effective temperature. Figure 4(b) shows a considerable deviation from linear behavior, even for small interaction strengths.

Figure 4(c) shows that, consistent with our previous discussion, irrespective of the choice of bath spectral function, the quantity $J/(I\omega_0)$, for $\chi \gg \Omega_0$, shows a data collapse and goes as $\sim\sqrt{T_1/\omega_0}$ for $T_1 \gg \omega_0$ (with r kept fixed).

Having discussed the scaling behavior of currents in detail, we now look into another important property of interacting systems, the rectification of current.

B. Rectification

Rectification of current is a generic behavior of nonlinear (interacting) systems in nonequilibrium. As we have seen, in a nonequilibrium setup, two kinds of currents through the system can be defined, the particle current and the energy current, and their rectification behavior can also differ considerably. To our knowledge, there has been no previous work where both particle and energy current rectification for a bosonic nonlinear system has been investigated. Also, note that rectification can only be observed beyond a linear response regime.

Since rectification occurs only for asymmetric system-bath coupling, we use the following definition to describe the degree of asymmetry:

$$\Gamma_1 = \Lambda(1-\gamma), \quad \Gamma_2 = \Lambda(1+\gamma), \tag{37}$$

where $0 \leqslant \gamma \leqslant 1$ is dimensionless. Given a value of asymmetry parameter γ, we define a measure of rectification as

$$R_I = \frac{I(\Delta T,\gamma) + I(-\Delta T,\gamma)}{I(\Delta T,\gamma=0)},$$
$$R_J = \frac{J(\Delta T,\gamma) + J(-\Delta T,\gamma)}{J(\Delta T,\gamma=0)}. \tag{38}$$

R_I and R_J are the particle and energy current rectifications. This measure of rectification is as used in Refs. [44,45]. Note that, by this definition, rectification is positive if higher current flows when the cold bath is more strongly coupled to the system. Also, R_I and R_J are zero when $\gamma = 0,1$. In our following discussion of rectification, we will primarily confine ourselves to the Ohmic baths [$s = 1$ in Eq. (5)].

The variation of R_I and R_J with γ is shown in Fig. 5. Irrespective of the strength of interaction strength, we notice that the maximum rectification occurs when $\gamma \approx 0.6$. The figure also shows that both particle and energy rectifications behave nonmonotonically with χ. For small χ, R_J is negative while R_I is positive, hence, the direction of energy rectification is opposite to particle rectification. For large χ, the rectification is the same as that obtained from NESB. In the NESB regime, particle and energy rectifications are the same, because particle

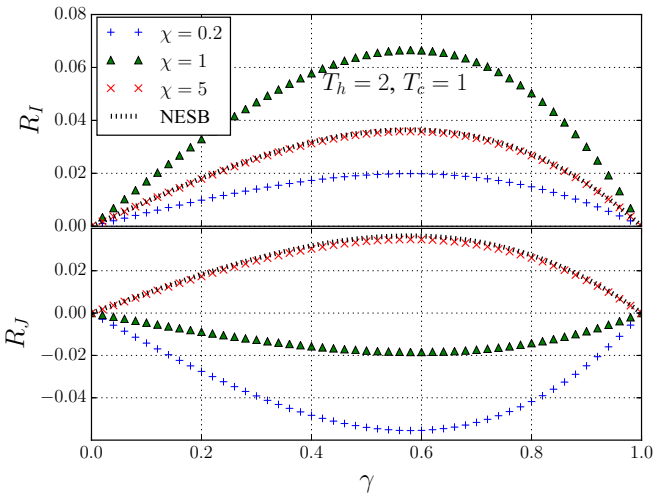

FIG. 5. The plot shows particle rectification R_I (top) and energy rectification R_J (bottom) as a function of asymmetry parameter γ for various values of interaction strength χ and Ohmic baths [$s = 1$ in Eq. (5)]. R_I and R_J are as defined in Eq. (38). The black dotted line corresponds to NESB. The rectfications become maximum when $\gamma \approx 0.6$. Also, rectification of both particle and energy currents show a nonmonotonic change with χ. Rectification for large χ matches with the NESB result. Energy rectification changes direction with increase in χ. Other parameters are as follows: $\varepsilon = 0.1$, $\omega_c = 1000$. All energy variables are measured in units of Ω_0, and time is measured in units of Ω_0^{-1}.

current is proportional to energy current. All these observations are consistent with our discussion of Fig. 3.

To concisely investigate the rectification behavior of the system as a function of the interaction strength and the temperatures, we again resort to the scaling variable T_1/ω_0 with r fixed at $r < 1$. The plots of R_I and R_J as a function of T_1/ω_0 for fixed r for Ohmic baths are shown in Fig. 6. We readily make the following observations.

First, for $\chi < \Omega_0$, rectification is small. For $\chi \gg \Omega_0$, there is data collapse as expected from the scaling of currents.

Second, where NESB matches the nonequilibrium SSBH model, there is small rectification. This can be understood from expression for currents in NESB regime given in Eq. (31). NESB result holds when $\chi \gg \Omega_0, T_1, T_2$. Therefore, in this regime $\omega_0 \gg T_1, T_2$. So the Bose distributions in Eq. (31) are exponentially small. Hence, $1 + \mathfrak{n}(\omega_0) \approx 1$. With this approximation, the expressions of currents in Eq. (31) become antisymmetric under interchange of hot and cold baths. Thus the NESB regime of the SSBH model gives very small rectification. Maximum particle rectification R_I is reached when $\omega_0 < T_1$, which is outside this regime.

Third, after the maximum, R_I gradually approaches zero with increase in T_1/ω_0. This is expected because, as we have seen before, at high temperatures, for Ohmic baths, the particle current eventually has the form, $I \approx A\Delta T$, which is antisymmetric under interchange of hot and cold baths. On the other hand, the corresponding NESB rectification (the dotted line in Fig. 6) continues to increase with T_1/ω_0, until it saturates to a high value. Thus, as an effect of having all energy levels, and not truncating at two levels, the particle rectification is suppressed at high temperatures.

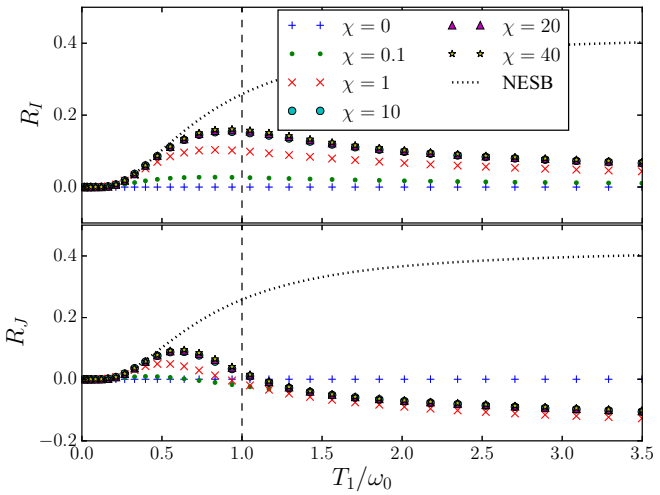

FIG. 6. The plot shows rectification of particle current (top panel) and of energy current (bottom panel) of SSBH model out-of-equilibrium for fixed $r = \frac{T_2}{T_1} = \frac{1}{3}$, for Ohmic baths [$s = 1$ in Eq. (5)]. $\omega_0 = \Omega_0 + \chi$. R_I and R_J are as defined in Eq. (38). The vertical dashed line indicates the positions of $T_1/\omega_0 = 1$. The dotted plots correspond to the NESB model. For $\chi \gg \Omega_0$, ($\Omega_0 = 1$), there is data collapse. Both R_I and R_J has a maximum for $\omega_0 < T_1$. $R_J = 0$ for $\omega_0 \approx T_1$. R_J shows reversal in direction of rectification beyond this point. Other parameters are as follows: $\varepsilon = 0.1$, $\omega_c = 1000$. All energy variables are measured in units of Ω_0 and time is measured in units of Ω_0^{-1}.

Fourth, and most interestingly, energy rectification R_J also has a peak for $\omega_0 < T_1$. However, $R_J = 0$ at $\omega_0 \approx T_1$. At this point, the particle rectification is still positive. So the system behaves as a particle rectifier and not as an energy or heat rectifier. Beyond that point, R_J changes sign. Thus the direction of rectification is reversed. With further increase in T_1/ω_0, energy rectification continues to grow in the reversed direction. Therefore, at high temperatures, the heat rectification occurs in the opposite direction to particle rectification and continues to grow as temperatures of both hot and cold baths are increased.

Note that all the above observations are for Ohmic baths [$s = 1$ in Eq. (5)]. Finally, we discuss the case of non-Ohmic baths. For super-Ohmic baths (i.e., for $s > 1$), both particle and energy currents show a reversal of direction of rectification. The reversal of energy rectification for super-Ohmic bath occurs at a lower value of T_1/ω_0 than that for the Ohmic bath. For sub-Ohmic baths (i.e., for $s < 1$), the reversal of energy rectification occurs at higher values of T_1/ω_0 than that for the Ohmic bath. The particle rectification does not show reversal for sub-Ohmic baths. For the constant bath, $s = 0$, neither particle nor energy rectification shows reversal. However, in all cases, both particle and energy rectifications vary nonmonotonically with the interaction strength.

VII. TIME DYNAMICS

Until now, we have discussed the properties of the NESS of the out-of-equilibrium SSBH model. In this section, we look at the transient time dynamics of the various physical quantities we have so far calculated in NESS.

To do this, we revert to the equation for time evolution of ρ_n, Eq. (10). The equation can be rewritten and solved in the form

$$\frac{\partial \tilde{\rho}(t)}{\partial t} = -\varepsilon^2 M \tilde{\rho}(0) \Rightarrow \tilde{\rho}(t) = e^{-\varepsilon^2 M t} \tilde{\rho}(0), \tag{39}$$

where $\tilde{\rho}$ is an infinite-dimensional column vector containing diagonal elements of the density matrix and M is a infinite-dimensional non-Hermitian square matrix containing the entries of Eq. (10). M has the form

$$M = \begin{bmatrix} C_0 + D_0 & -D_1 & 0 & \dots & \dots & \dots \\ -C_0 & C_1 + D_1 & -D_2 & 0 & \dots & \dots \\ 0 & -C1 & C_2 + D_2 & -D_3 & 0 & \dots \\ \vdots & \ddots & \ddots & \ddots & \ddots & \ddots \end{bmatrix}, \tag{40}$$

where C_n and D_n are as defined in Eq. (11). Note that the matrix M has the form of a Markov matrix. The sum of each column is zero ($D_0 = 0$ by definition). This corresponds to the fact that the trace of the density matrix is preserved, i.e., $\sum_n \rho_n = 1$.

To calculate the time dynamics, we choose an initial state with no particles in the system, i.e., initially, $\rho_0(0) = 1$ and $\rho_n(0) = 0\ \forall n \neq 0$. The Eq. (39) is used to numerically obtain the time evolution. Even though the matrices involved are infinite dimensional, for given interaction χ and temperatures T_1 and T_2, only a finite number of levels, determined by the ratio of the temperatures and the interaction, effectively contribute. Thus, starting from a finite matrix size, a convergence is reached as the matrix size is increased. Smaller interaction and higher temperatures require larger matrix sizes. A subtle point to note is that if the matrix M is truncated at any finite size, say, p, then the constraint that the sum of each column should be zero is not satisfied for the pth column, unless $C_p = 0$. Consequently, the matrix M can be truncated at size p only if $C_p \ll D_p$.

Since we are using Redfield equation under Born-Markov approximation to obtain transient time dynamics, we need to be careful in choosing the observation times. This is because, as mentioned in Sec. III, Markov approximation is valid only when observation times are much larger than the time for decay of bath correlation functions. We have made some estimates (similar to that in Ref. [52]), which indicate that the bath relaxation times are indeed much smaller than the observational transient times of our interest.

Time dynamics of physical quantities $\langle \hat{N}(t) \rangle$, $\langle \hat{H}_s(t) \rangle$, $I(t)$, $J(t)$ for Ohmic baths [$s = 1$ in Eq. (5)] are shown in Fig. 7, where $I_1(t)$ and $J_1(t)$ are, respectively, particle and energy currents from the left bath into the system. (Before reaching steady state, the currents from the left and right baths are not the same.) Similar time dynamics, but for bosonic system of two sites without interactions, was calculated in Ref. [52]. We observe that, unlike the two site noninteracting case in Ref. [52], here, the currents show no oscillations. More interestingly, we also observe that the time to reach steady state, called t_{ss} hereafter, decreases with increase in the interaction. In the following, we investigate the dependence of t_{ss} on setup parameters more carefully.

We note from the solution of $\tilde{\rho}(t)$ in Eq. (39) that time can be scaled as $\varepsilon^2 t$. It follows that $t_{ss} \propto \varepsilon^{-2}$. Thus, the time to

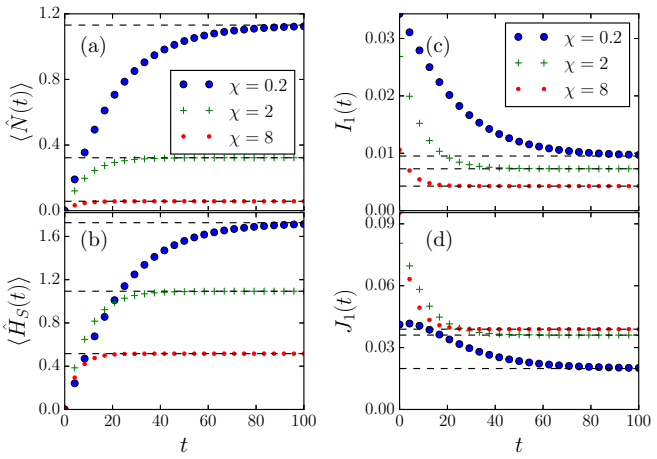

FIG. 7. The figure shows time dynamics of (a) average occupation, $\langle N(t) \rangle$; (b) average energy, $\langle H_s(t) \rangle$; (c) particle current from left bath, $I_1(t)$; and (d) energy current from left bath, $J(t)$, for various values of interaction strength and for a temperature bias $T_1 = 4$ and $T_2 = 2$ for Ohmic baths [$s = 1$ in Eq. (5)]. All physical quantities demonstrate a nonunitary evolution towards a steady state. The approach to steady state is faster for higher interactions. Since physical quantities plotted here are diagonal in the eigenbasis of the system Hamiltonian, none of them show oscillations with time. Other parameters are $\Omega_0 = 1$, $\varepsilon = 0.1$, $\Gamma_1 = 0.4$, $\Gamma_2 = 1.6$, $\omega_c = 1000$. All energy variables are measured in units of Ω_0, and time is measured in units of Ω_0^{-1}.

reach steady state increases as system-bath coupling becomes weaker.

It is also clear from Eq. (39) that the steady state is given by the eigenvector of the matrix M corresponding to zero eigenvalue. The fact that a unique steady state is reached in long times then implies that all other eigenvalues of the M have a positive real part. Interestingly, we have found in our numerical computation that the eigenvalues of M are all real (and hence no oscillations in time). The smallest nonzero eigenvalue then gives a measure of t_{ss}. So, we define

$$t_{ss} \equiv \frac{1}{\varepsilon^2 \lambda_1}, \tag{41}$$

with λ_1 being the smallest nonzero eigenvalue of M.

Even though t_{ss} cannot be calculated for all setup parameters analytically, in two limiting cases, analytical results can be obtained. The first case corresponds to the NESB regime $\chi \gg \Omega_0, T_1, T_2$. In this case, $C_1 \ll D_1$, only two levels effectively contribute and matrix M has the form

$$M \approx \begin{bmatrix} C_0 & -D_1 \\ -C_0 & D_1 \end{bmatrix}. \tag{42}$$

The nonzero eigenvalue of M is

$$\lambda_1 = [\varepsilon^2 t_{ss}]^{-1} \approx C_0 + D_1 = \sum_{\ell=1}^{2} \mathcal{J}_\ell(\omega_0)[2\mathfrak{n}_\ell(\omega_0) + 1]. \tag{43}$$

The time to reach steady state therefore also depends on the temperatures of the baths. However, for large $\omega_0 = \Omega_0 + \chi$, the Bose distributions are exponentially small. Thus, for $\chi \gg \Omega_0, T_1, T_2$ and for a general bath of the form given in Eq. (5),

$$t_{ss} \approx \frac{1}{\varepsilon^2 \chi^s (\Gamma_1 + \Gamma_2)}, \tag{44}$$

which is independent of the temperatures of the baths. We also see that, for constant baths [$s = 0$ in Eq. (5)], t_{ss} is independent of interaction strength. For other baths, t_{ss} decreases with increase of interaction strength as a power law.

The second case where t_{ss} can be analytically calculated corresponds to the linear system, $\chi = 0$. In this case, C_n does not decay with n [Eq. (11) for $\chi = 0$] and hence the matrix M cannot be truncated at any finite size. So, the above method of finding t_{ss} fails. However, since, in this case, we have a noninteracting system, we can find t_{ss} directly from the evolution equation for $\langle \hat{N}(t) \rangle$. The evolution equation for $\langle \hat{N}(t) \rangle$ can be obtained from Eq. (27) by setting $\chi = 0$. The resulting equation can be written and solved in the form

$$\frac{d\langle \hat{N}(t) \rangle}{dt} = -\varepsilon^2 \langle \hat{N}(t) \rangle \sum_{\ell=1}^{2} \mathcal{J}_\ell(\Omega_0) + \varepsilon^2 \sum_{\ell=1}^{2} \mathcal{J}_\ell(\Omega_0)\mathfrak{n}_\ell(\Omega_0)$$

$$\Rightarrow \langle \hat{N}(t) \rangle = (\langle \hat{N}(0) \rangle - N_{ss}) e^{-\varepsilon^2 t \sum_{\ell=1}^{2} \mathcal{J}_\ell(\Omega_0)} + N_{ss} \tag{45}$$

with $N_{ss} = [\sum_{\ell=1}^{2} \mathcal{J}_\ell(\Omega_0)\mathfrak{n}_\ell(\Omega_0)]/[\sum_{\ell=1}^{2} \mathcal{J}_\ell(\Omega_0)]$ being the NESS occupation. From above equation, it is clear that for $\chi = 0$, the t_{ss} is given by

$$t_{ss} = \frac{1}{\varepsilon^2 \sum_{\ell=1}^{2} \mathcal{J}_\ell(\Omega_0)}. \tag{46}$$

This is again independent of the temperatures of the baths.

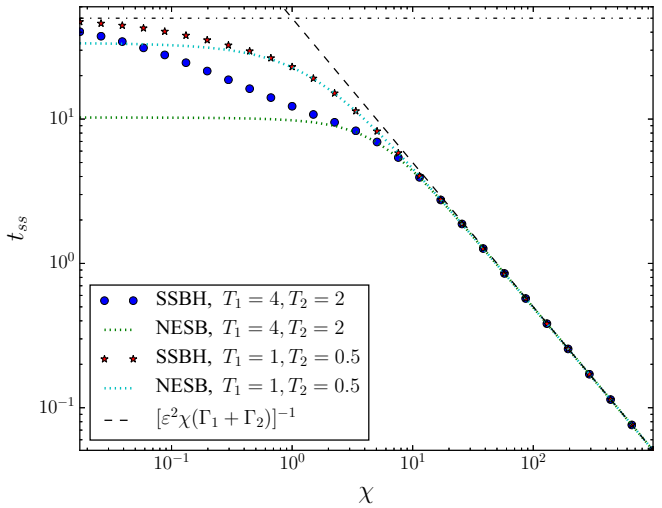

FIG. 8. The figure shows a log-log plot of time to reach NESS, t_{ss} [as defined in Eq. (41)] as a function of interaction strength χ for Ohmic baths [$s = 1$ in Eq. (5)]. The horizontal dash-dotted line corresponds to $[\varepsilon^2 \sum_{\ell=1}^{2} \mathcal{J}_\ell(\Omega_0)]^{-1}$, which is the t_{ss} for the linear ($\chi = 0$) system. For large χ, $t_{ss} \approx [\varepsilon^2 \chi(\Gamma_1 + \Gamma_2)]^{-1}$, and this is indicated by the dashed line. For intermediate χ, t_{ss} depends on the temperatures of the hot and cold baths. Other parameters are $\Omega_0 = 1$, $\varepsilon = 0.1$, $\Gamma_1 = 0.4$, $\Gamma_2 = 1.6$, $\omega_c = 1000$. All energy variables are measured in units of Ω_0, and time is measured in units of Ω_0^{-1}.

Except for these two limiting cases, t_{ss} needs to be found numerically using the definition Eq. (41). Figure 8 shows log-log plot of numerically obtained t_{ss} as a function of interaction strength χ for Ohmic baths for two different choices of temperatures of hot and cold baths. It is seen that, except for the limiting cases, t_{ss} depends on the temperatures of the baths. The limiting cases show the behavior discussed above.

VIII. CONCLUSION

We have investigated a system consisting of a single bosonic site with Bose-Hubbard interaction weakly coupled to two bosonic baths at different temperatures. We have used the Redfield QME method to obtain analytical results beyond linear response regime. Below, we summarize our main findings and their potential applications.

We have found an analytical result for the population density (diagonal elements of the density matrix in the eigenbasis of system Hamiltonian) of the system in NESS [Eq. (13)]. This has further allowed us to find various physical observables like average occupation and energy, as well as the particle and energy currents in NESS. We have then analytically found interesting scaling behavior of the physical observables. Our main finding in this respect is that the high-temperature behavior of the system can be described in terms of an effective temperature [Eq. (20)]. Then, it follows that, with the ratio r of the temperatures of cold and hot baths fixed, there occurs a data collapse for various strengths of interaction χ, when physical observables of the system are plotted in terms of the scaling variable T_1/ω_0 (Figs. 2, 4, and 6). The scaling behaviours hold for a general choice of bath spectral functions of the form given in Eq. (5). We have also found very interesting rectification behavior of the system. The most interesting finding is that, for Ohmic and sub-Ohmic baths [$0 < s \leqslant 1$ in Eq. (5)], the energy current shows a reversal in the direction of rectification (Fig. 6). It follows that there is a nonzero strength of interaction strength, ($\chi \approx T_1 - \Omega_0$, for Ohmic baths), where energy or heat rectification is zero. At this point, the system behaves as a particle rectifier but not as a heat rectifier. For super-Ohmic baths [$s > 1$ in Eq. (5)], both particle and energy currents show reversal in direction of rectification. For constant baths [$s = 0$ in Eq. (5)], there is no change in direction of rectification for both particle and energy currents. Therefore careful engineering of baths can lead to various interesting rectification behavior of the system. Such phenomena can be potentially used to create quantum devices, such as optical diodes. Reversal of direction of thermal rectification of a quantum system has also been previously theoretically seen for a Heisenberg spin chain out of equilibrium [53]. Further, we have computed nonunitary time dynamics of various physical quantities (Fig. 7). We found that, except for constant baths, the time to reach steady state is shorter for higher interactions and higher system-bath couplings. For constant baths, with increase in interaction, the time to reach steady state approaches a constant independent of the strength of interaction. For large χ, the time to reach steady state goes as $t_{ss} \sim [\varepsilon^2 \chi^s]^{-1}$ for a general choice of bath spectral functions of the form given in Eq. (5). All our results also are consistent with the linear, $\chi = 0$ (harmonic oscillator), case, as well as the NESB, $\chi \gg \Omega_0, T_1, T_2$, case.

Our results are experimentally relevant in quantum hybrid systems, where a single-site Bose-Hubbard model can be realized, as well as in molecular junction systems, where our setup describes a model for anharmonic junctions. Future work includes going to a strong system-bath coupling regime, as well as to generalize to nonequilibrium interacting systems of more than one site, such as the nonequlibrium Bose Hubbard chain [54–57] and the Jaynes-Cummings Hubbard model [58].

ACKNOWLEDGMENTS

A.D. acknowledges support from the Indo-Israel joint research Project No. 6-8/2014(IC) and from the French Ministry of Education through the Grant ANR (EDNHS).

[1] S. Schmidt and J. Koch, Ann. Phys. **525**, 395 (2013).
[2] Z. L. Xiang, S. Ashhab, J. Q. You, and F. Nori, Rev. Mod. Phys. **85**, 623 (2013).
[3] I. M. Georgescu, S. Ashhab, and F. Nori, Rev. Mod. Phys. **86**, 153 (2014).
[4] I. Buluta and F. Nori, Science **326**, 108 (2009).
[5] G. Kurizkia, P. Bertetb, Y. Kubob, K. Molmerc, D. Petrosyand, P. Rablf, and J. Schmiedmayer, Proc. Natl. Acad. Sci. USA **112**, 3866 (2015).
[6] I. N. Hincks, C. E. Granade, T. W. Borneman, and D. G. Cory, Phys. Rev. Appl. **4**, 024012 (2015).
[7] K. L. Hur, L. Henriet, A. Petrescu, K. Plekhanov, G. Roux, and M. Schiró, C. R. Physique **17**, 808 (2016).
[8] A. A. Houck, H. E. Türeci, and J. Koch, Nat. Phys. **8**, 292 (2012).
[9] M. R. Delbecq, V. Schmitt, F. D. Parmentier, N. Roch, J. J. Viennot, G. Féve, B. Huard, C. Mora, A. Cottet, and T. Kontos, Phys. Rev. Lett. **107**, 256804 (2011).
[10] K. Saito and T. Kato, Phys. Rev. Lett. **111**, 214301 (2013).
[11] J.-H. Jiang, M. Kulkarni, D. Segal, and Y. Imry, Phys. Rev. B **92**, 045309 (2015).
[12] T. Werlang, M. A. Marchiori, M. F. Cornelio, and D. Valente, Phys. Rev. E **89**, 062109 (2014).
[13] K. Joulain, J. Drevillon, Y. Ezzahri, and J. Ordonez-Miranda, Phys. Rev. Lett. **116**, 200601 (2016).
[14] B. Xu and Y. Dubi, J. Phys.: Condens. Matter **27**, 263202 (2015).
[15] D. M.-T. Kuo and Y.-c. Chang, Phys. Rev. B **81**, 205321 (2010).
[16] K. Ono, D. G. Austing, Y. Tokura, and S. Tarucha, Science **297**, 1313 (2002).
[17] D.-W. Wang, H.-T. Zhao, M.-J. Guo, J.-X. Zhang, J. Evers, and S.-Y. Zhu, Phys. Rev. Lett. **110**, 093901 (2013).
[18] H. Z. Shen, Y. H. Zhou, and X. X. Yi, Phys. Rev. A **90**, 023849 (2014).
[19] E. Mascarenhas, D. Gerace, D. Valente, S. Montangero, D. Auffèves, and M. F. Santos, Europhys. Lett. **106**, 54003 (2014).

[20] M. E. Kimchi-Schwartz, L. Martin, E. Flurin, C. Aron, M. Kulkarni, H. E. Türeci, and I. Siddiqi, Phys. Rev. Lett. **116**, 240503 (2016).
[21] A. J. Hoffman, S. J. Srinivasan, S. Schmidt, L. Spietz, J. Aumentado, H. E. Türeci, and A. A. Houck, Phys. Rev. Lett. **107**, 053602 (2011).
[22] S. Schmidt, D. Gerace, A. A. Houck, G. Blatter, and H. E. Türeci, Phys. Rev. B **82**, 100507(R) (2010).
[23] A. Nunnenkamp, J. Koch, and S. M. Girvin, New J. Phys. **13**, 095008 (2011).
[24] I. Carusotto, D. Gerace, H. E. Tureci, S. De Liberato, C. Ciuti, and A. Imamoglu, Phys. Rev. Lett. **103**, 033601 (2009).
[25] D. Gerace, H. E. Türeci, A. Imamoglu, V. Giovannetti, and R. Fazio, Nat. Phys. **5**, 281 (2009).
[26] Y. Y. Liu, J. Stehlik, C. Eichler, M. J. Gullans, J. M. Taylor, and J. R. Petta, Science **347**, 285 (2015).
[27] P. Roushan *et al.*, Nat. Phys., doi:10.1038/nphys3930 (2016).
[28] M. Boissonneault, J. M. Gambetta, and A. Blais, Phys. Rev. A **79**, 013819 (2009).
[29] M. J. Hartmann and M. B. Plenio, Phys. Rev. Lett. **99**, 103601 (2007).
[30] Z. Ling, L. Zhong-Ju, Y. Wei-Bin, and Mu. Qing-Xia, Chin. Phys. B **20**, 074205 (2011).
[31] D. Schwarzer, P. Kutne, C. Schröder, and J. Troe, J. Chem. Phys. **121**, 1754 (2004).
[32] R. Y. Wang, R. A. Segalman, and A. Majumdar, Appl. Phys. Lett. **89**, 173113 (2006).
[33] T. Meier, F. Menges, P. Nirmalraj, H. Hölscher, H. Riel, and B. Gotsmann, Phys. Rev. Lett. **113**, 060801 (2014).
[34] M. D. Losego, M. E. Grady, N. R. Sottos, D. G. Cahill, and P. V. Braun, Nat. Mater. **11**, 502 (2012).
[35] N. I. Rubtsova, C. M. Nyby, H. Zhang, B. Zhang, X. Zhou *et al.*, J. Chem. Phys. **142**, 212412 (2015).
[36] N. I. Rubtsova and I. V. Rubtsov, Annu. Rev. Phys. Chem. **66**, 717 (2015).
[37] D. Segal and B. K. Agarwalla, Annu. Rev. Phys. Chem. **67**, 185 (2016).
[38] P. D. Drummond and D. F. Walls, J. Phys. A **13**, 725 (1980).
[39] F. Haake, H. Risken, C. Savage, and D. Walls, Phys. Rev. A **34**, 3969 (1986).
[40] G. J. Milburn and C. A. Holmes, Phys. Rev. Lett. **56**, 2237 (1986).
[41] H. Risken, C. Savage, F. Haake, and D. F. Walls, Phys. Rev. A **35**, 1729 (1987).
[42] R. Alicki, Phys. Rev. A **40**, 4077 (1989).
[43] F. X. Kärtner and A. Schenzle, Phys. Rev. A **48**, 1009 (1993).
[44] D. Segal and A. Nitzan, Phys. Rev. Lett. **94**, 034301 (2005).
[45] D. Segal and A. Nitzan, J. Chem. Phys. **122**, 194704 (2005).
[46] D. Segal, Phys. Rev. B **73**, 205415 (2006).
[47] T. Ruokola and T. Ojanen, Phys. Rev. B **83**, 045417 (2011).
[48] D. Segal, Phys. Rev. E **90**, 012148 (2014).
[49] J. Thingna, J. L. García-Palacios, and J.-S. Wang, Phys. Rev. B **85**, 195452 (2012).
[50] D. He, J. Thingna, J.-S. Wang, and B. Li, Phys. Rev. B **94**, 155411 (2016).
[51] A. Dhar, K. Saito, and P. Hänggi, Phys. Rev. E **85**, 011126 (2012).
[52] A. Purkayastha, A. Dhar, and M. Kulkarni, Phys. Rev. A **93**, 062114 (2016).
[53] L. Zhang, Y. Yan, C. Q. Wu, J. S. Wang, and B. Li, Phys. Rev. B **80**, 172301 (2009).
[54] G. Kordas, D. Witthaut, and S. Wimberger, Ann. Phys. (Berlin) **527**, 619 (2015).
[55] A. Biella, L. Mazza, I. Carusotto, D. Rossini, and R. Fazio, Phys. Rev. A **91**, 053815 (2015).
[56] M. J. Hartmann, Phys. Rev. Lett. **104**, 113601 (2010).
[57] T. Mertz, I. Vasić, M. J. Hartmann, and W. Hofstetter, Phys. Rev. A **94**, 013809 (2016).
[58] S. Schmidt and G. Blatter, Phys. Rev. Lett. **103**, 086403 (2009).